12^{th} International Conference on Fracture Mechanics of Concrete and Concrete Structures
FraMCoS-12
B.L.A. Pichler, Ch. Hellmich, P. Preinstorfer (Eds)

https://doi.org/10.21012/FC12.1193
MS10-1:4

EXPLORING INDUCED HETEROGENEITY IN ELASTIC DISCRETE MECHANICAL MODELS

JAN RAISINGER*, QIWEI ZHANG‡ AND JOHN E. BOLANDER‡, JAN ELIÁŠ*

* Brno University of Technology, Institute of Structural Mechanics
Brno 60200, Czech Republic
e-mail: jan.raisinger@vut.cz, jan.elias@vut.cz

† University of California, Department of Civil and Environmental Engineering
Davis, CA, United States
e-mail: qvvzhang@ucdavis.edu, jebolander@ucdavis.edu

Key words: Discrete Model, Stress Oscillations, Concrete Mesoscale, Heterogeneity, Randomization, Elasticity

Abstract. Mesoscale discrete lattice models offer a direct way to incorporate the heterogeneous microstructure of concrete and other geomaterials efficiently, using vector-based constitutive laws with homogeneous material parameters. These models exhibit stress oscillations, which, if deemed non-physical, can be suppressed using methods such as auxiliary stress projection or deviatoric-volumetric decomposition to produce homogeneous elastic stress fields. This study examines the elastic behavior of the homogenized models with controlled heterogeneity introduced via spatial randomization of material parameters, with an emphasis on the replication of the oscillations in the non-homogenized discrete model. Simulations with varying degrees of spatial correlation under different macroscopic loading conditions reveal that the original stress oscillations are best replicated with spatially independent randomization. However, none of the techniques fully reproduce the original oscillations.

1 INTRODUCTION

Discrete models, particularly particle-based lattice models, have proven effective in modeling the fracture behavior of materials with heterogeneous microstructures [1, 2, 3]. Advanced models like the Lattice Discrete Particle Model (LDPM) excel in simulating various structural configurations and loading scenarios [4, 5]. Modern approaches also couple mechanical models with other physical or chemical phenomena [6, 7].

Unlike continuum methods, particle-based models use vectorial constitutive relations at particle contacts, often resulting in stress oscillations [8]. These oscillations, shaped by *physical* discretization of the domain based on material heterogeneity [9], can aid in simulating phenomena like concrete compressive failure [10], though this approach has deficiencies such as restricted macroscopic Poisson's ratio [11]. *Non-physical* discretization, combined with methods like volumetric-deviatoric decomposition [12] or auxiliary stress projection [13], eliminates these oscillations but reduces the model's ability to represent heterogeneity.

This study builds on previous work [8], exploring whether controlled randomization can recover elastic stress oscillations typical for *physical* discretization.

2 SIMULATION FRAMEWORK

The three-dimensional discrete models used here represent concrete at the mesoscale, distinguishing aggregate inclusions and cementitious binders as separate phases. Aggregates are randomly distributed based on specified volume fractions and size distributions, with Delaunay triangulation and power tessellation defining rigid bodies and contact elements. Each contact element, connecting two nodes, has a defined area, length, and a local reference system (N, M, L), with displacements and rotations forming the degrees of freedom.

The models are governed by balance equations for linear and angular momentum, which sum element reactions ($\boldsymbol{t}$) and moments of these tractions, with constitutive relations defining elastic behavior and kinematic equation providing strain measures ($\boldsymbol{e}$). Three constitutive model variants are considered.

2.1 Constitutive models

Variant S: A standard model with elastic parameters E_0 and α with approximate relations to macroscopic elastic parameters E and ν. Parameter α determines the macroscopic Poisson's ratio. The orthogonal traction components are

$$t_N = E_0 e_N \quad t_M = \alpha E_0 e_M \quad t_L = \alpha E_0 e_L \quad (1)$$

This constitutive model results in local oscillations of macroscopic stress [8].

Variant V: This model developed by Cusatis, Rezakhani und Schauffert [12] features elastic constants E_V and E_D with exact relations to E and v. The tractions read

$$\begin{aligned} t_N &= E_D e_N + (E_V - E_D)\,\varepsilon_V \\ t_M &= \alpha E_D e_M \qquad t_L = E_D e_L \end{aligned} \quad (2)$$

where volumetric strain ε_V is obtained as an average from contact simplices.

Variant H: The third model, developed in Refs. [13, 14], follows the standard model from Eq. (1) with $\alpha = 1$. The parameter E_0 is then directly equal to E, such a model exhibits no stress oscillations, and the Poisson's ratio is zero [9]. To achieve nonzero macroscopic Poisson's ratio, eigenstrain at each element modifying its tractions is computed from the estimated macroscopic stress tensors at the element nodes. Through iterative loops, global balance is found. The macroscopic values E and ν are the user-defined parameters of this model.

Variants V and H yield elastically homogeneous models with the same macroscopic properties but differ in the input elastic parameters.

2.2 Periodic RVE model geometry

The model is constructed with periodic geometry in a cube of size l_{RVE} called the Representative Volume Element (RVE). Spheres, with sizes ranging from 4 to 10 mm in diameter according to the Fuller curve, are randomly placed ensuring no overlap, afterwards, the periodic power tesselation is performed.

Periodic boundary conditions are applied together with a macroscopic strain tensor $\boldsymbol{\varepsilon}$, controlling displacements between primary and dependent nodes, with one primary node's displacement fixed to prevent rigid-body translations.

100 periodic models of size $l_{\text{RVE}} = 100$ mm with differing internal geometry with 19900 elements and 3400 nodes on average were used for nodal stress field analysis. An example of the model is shown in Fig. 1, contact facets are visible on the left-hand side, and on the right-hand side the lattice elements which are colored by σ_{xx} stress tensor component under pure shear load are shown.

All simulations are conducted using the open-source software OAS available at `https://gitlab.com/kelidas/OAS`, employing a modified Newton-Raphson iteration solver in steady state.

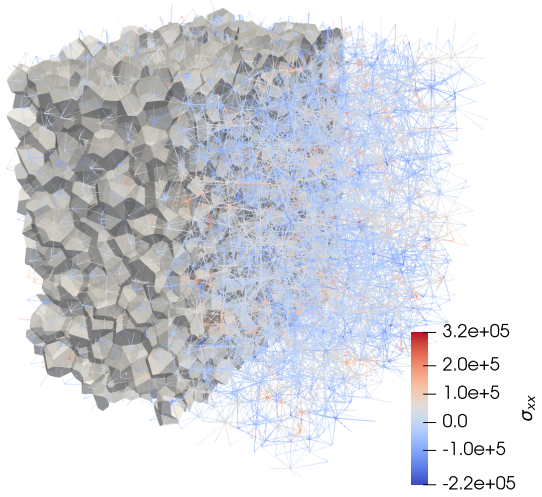

Figure 1: Contact facets and discrete elements in an RVE of size $l_{\text{RVE}} = 100$mm. The elements are colored by the nodal stress component σ_{xx}.

3 CONTROLLED HETEROGENEITY

In the following simulations, the standard (S) material is used with parameter values $E_0 = 40$ GPa and $\alpha = 0.24$ typical for ordinary concrete. The effective macroscopic values E_{eff}, ν_{eff} are found for each RVE by applying strain load in six linearly independent directions and numerical fitting of theoretical isotropic stiffness tensor.

The volumetric-deviatoric split material (V) uses the effective values from the S material $E_D = E_{\text{eff}}/(1+\nu_{\text{eff}})$ and $E_V = E_{\text{eff}}/(1-2\nu_{\text{eff}})$. To introduce heterogeneity, these values were randomized by randomly drawing E_D from a uniform distribution with bounds $(1-\eta)\mu_D$ and $(1+\eta)\mu_D$ where μ_D is the mean value. Such material variant is denoted V-RD. Because of local parallel and serial connections of elements, μ_D is computed for each RVE separately so that its effective parameters match those of the standard material.

The H material uses parameters $E = E_{\text{eff}}$, $\nu = \nu_{\text{eff}}$. They were randomized by three different approaches. Variant H-R draws E and ν for each element independently from uniform distributions with mean values μ_E and μ_ν and width parameters η_E and η_ν. The mean values are calculated analogically to those in V-RD variant.

Variant H-RD randomizes only the deviatoric component of the material stiffness, E_D, keeping the volumetric part constant. For each element, E and ν values are calculated from E_D value randomly drawn from a uniform distribution with μ_D and η_D parameters.

Lastly, the H-RF variant generates E and ν independently but spatially correlated as realizations of random fields with uniform marginal distributions defined by widths η and mean values μ. Random fields are generated via the Karhunen–Loève expansion [15, 16, 17]. Periodic metric ensures periodicity of the generated Gaussian random fields, which are transformed to non-Gaussian space using an approximation of Nataf transformation from Ref. [18]. Correlation length ℓ_c is a user-defined parameter of the Gaussian autocorrelation function.

4 STRESS FIELDS COMPARISON

The RVEs with different elastic constitutive model variants are subjected to macroscopic strain loading. Tensorial stresses are calculated for each rigid body node. Thanks to the model's perfect periodicity, stress field ergodicity is ensured, meaning statistical sampling across space and RVE realizations is equivalent. A statistical assessment of the stress fields is presented for different loading scenarios. To compare the stress fields of the different materials, the Δ_{hist} value is introduced. It measures the distance of two histograms of nodal stress components as Euclidian distance $\Delta_{\text{hist}} = \pm\sqrt{\sum_{i=1}^{n}\left[h_1(i)-h_2(i)\right]^2}$ where $h_1(i)$ and $h_2(i)$ is the frequency of the ith bin in the first and the second histogram, respectively, and n is the number of bins, which is identical ($n = 30$) in all histograms. The sign indicates which distribution is wider and which is narrower. A negative sign means the peak of the first material is larger and vice versa.

4.1 Loading Scenarios

In the *Load 1* scenario the RVEs are loaded with purely volumetric macroscopic strain tensor where $\varepsilon_{ij} = \varepsilon_V \delta_{ij}$, with δ_{ij} being the Kro-

necker delta and $\varepsilon_V = 1.5 \times 10^{-5}$ being a scalar representing volumetric strain.

The *Load 2* and *Load 3* scenarios are variants of purely deviatoric loads. The nonzero values of the macroscopic strain tensor $\{\varepsilon_{xx}, \varepsilon_{yy}, \varepsilon_{zz}, \varepsilon_{yz}, \varepsilon_{xz}, \varepsilon_{xy}\}$ are $\varepsilon_{yz} = \varepsilon_{xz} = \varepsilon_{xy} = 1.5 \times 10^{-5}$ for *Load 2* and $\varepsilon_{xy} = 2.6 \times 10^{-5}$ for *Load 3*. Both loads have the same value of equivalent strain ε_{eq} computed analogically to the Von Mises stress value.

Lastly, *Load 4* is the linear combination of *Load 1* and *Load 3*, having the same ε_V and ε_{eq} respectively.

4.2 *Load 1* results

The mean values of the stress components under the purely volumetric loading are constant between the nonrandomized models (S, H, V) and the variant with only deviatoric stiffness randomization (H-RD, V-RD). The standard variation of the components is close to zero for all these variants, slight differences caused by the iterative calculation are seen for H-RD and V-RD materials. However, in the H-R variant, the stress is not constant and oscillates in space with the mean values converging to those of the other materials with the number of samples.

4.3 *Load 2* and *Load 3* results

Under the purely deviatoric loading, only the H and V variants produce homogenous stress fields. The other variants exhibit stress oscillations, which were studied in the original reference system xyz and rotated reference system 123 corresponding to the principal directions of the macroscopic strain tensors. The uniform distribution width parameters of the H-R material variant $\eta_E = \eta_D$, which would produce stress oscillations similar to those in the S variant, therefore having Δ_{hist} value between S and H-R variants minimal for all stress tensor components, were sought after.

The $\eta_E = \eta_\nu = 0.7$ parameters were found to produce fields with low Δ_{hist} in all coaxial stress directions under *Load 2*. However, when the same stress fields were inspected in the principal directions, the Δ_{hist} changed significantly, and no η_E, η_ν could minimize all Δ_{hist} simultaneously. Histograms of σ_{yz} and σ_{23} are shown in Fig. 2. From the σ_{yz} component its mean value is subtracted for better comparison. The variation in the H-R histograms based on the chosen reference system is due to the relationships between the stress tensor components. Pearson correlation matrices show that while in S material the correlations are negligible ($< |\sim \pm 0.1|$), in the H-R material they are significant ($\approx 0.3 \sim 0.6$).

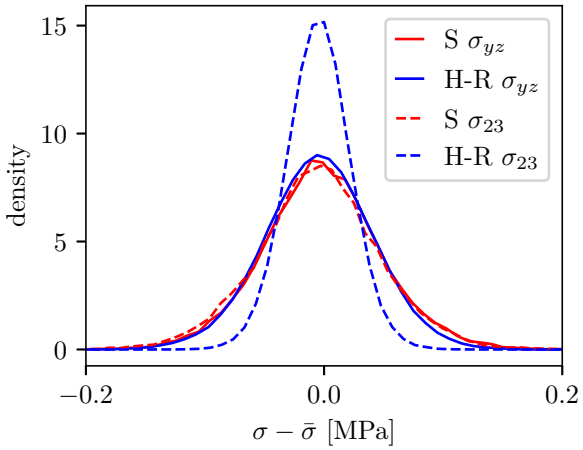

Figure 2: Histograms of σ_{yz} and σ_{23} stress components

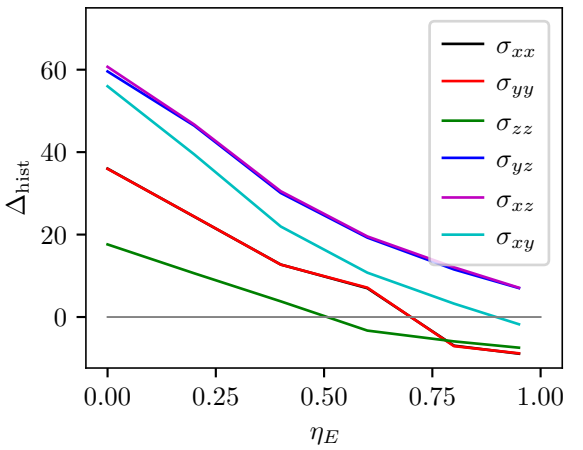

Figure 3: Histogram distance Δ_{hist} between S and H-R material variants for different η_E. $\eta_\nu = 0.7$ is constant.

For the *Load 3*, which represents a different deviatoric load type, no η_E, η_ν values were

found that would minimize the Δ_{hist} in either reference system. This is demonstrated in Fig. 3, which shows the Δ_{hist} values for different η_E during *Load 3*. The η_ν has no significant effect on the stress oscillations. The Δ_{hist} for both *Load 2* and *Load 3* and both reference systems for $\eta_E = \eta_\nu = 0.7$ can be seen in Tables 1 and 2.

The H-RD and V-RD variants show similar stress oscillation characteristics, succeeding in minimizing Δ_{hist} only in the specific case of *Load 2* and coaxial stress directions.

The H-RF material was compared to the S material in terms of variograms. The $\eta_E = \eta_\nu = 0.7$ values were used for the marginal uniform distributions. The variogram of σ_{xx} is shown in Fig. 4. It can be seen that the H-R and V-RD variants show similar spatial dependency to the S material. The H-RF martial exhibits significantly lower variances decreasing with a higher correlation length ℓ_c.

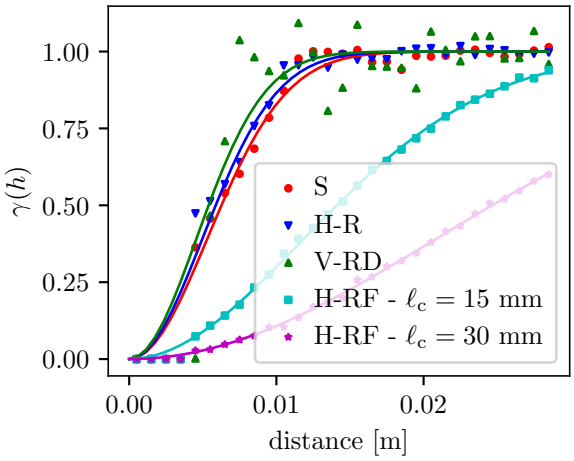

Figure 4: Variogram of σ_{xx} under *Load 2*

Table 1: Coaxial stress components Δ_{hist} values between H-R and S variant under *Load 2* and *Load 3*

Load	σ_{xx}	σ_{yy}	σ_{zz}	σ_{yz}	σ_{xz}	σ_{xy}
2	2.1	2.1	2.1	1.4	1.3	1.4
3	1.9	1.7	−3.1	12.7	12.9	4.9

Table 2: Principal stress components Δ_{hist} values between H-R and S variant under *Load 2* and *Load 3*

Load	σ_{11}	σ_{22}	σ_{33}	σ_{23}	σ_{13}	σ_{12}
2	1.8	1.7	−3.0	14.2	14.5	5.3
3	−3.3	−3.6	18.1	9.8	9.1	18.2

4.4 *Load 4* results

In the case of *Load 4*, which is a combination of *Load 1* and *Load 3*, the material's linear elasticity ensures that the results are simply the sum of the results from the individual component loads. The H-RD and V-RD materials therefore produce the same oscillations as in the case of *Load 3*. This also shows that the H-R material cannot replicate the standard material for varying loading types, as the volumetric component differently affects the resulting oscillations.

Due to the difference in the stress homogenization procedure of V and H material, when using the same randomization characterized by the η_D value for the H-RD and V-RD variants, the former produces oscillations with larger variability. Also, the ratio of the variability between the stress components is slightly different.

5 CONCLUSIONS

By applying a stress homogenization methods a uniform local response of a discrete model with non-physical discretization is obtained. The volumetric-deviatoric decomposition of the constitutive model and the auxiliary stress projection method were implemented to obtain elastically homogeneous discrete models. Through spatial randomization of the elastic material parameters, the stress response can be heterogenized in a controlled manner. Different approaches to the randomization of their elastic parameters were introduced and the characteristics of the resulting stress oscillations were compared.

Significant challenges were found in replicating the stress field characteristics of the stan-

dard material. Under pure volumetric loading, both standard and homogenized materials produce homogeneous stress fields, the same applies when only the deviatoric part of the homogeneous constitutive model is randomized. Expectedly, when the volumetric part is also randomized, stress oscillations occur.

When a deviatoric component of the loading is present, both the standard and the randomized materials produce stress oscillations. However, no single randomization approach for homogenized materials successfully reproduces the statistical characteristics of stress fields observed in standard materials across all loading scenarios. Matching stress distributions depends heavily on the applied load, requiring repeated recalibration for different strain tensors. Furthermore, the standard material exhibits statistically independent stress components that randomized models fail to replicate, showing significant cross-correlation, which causes different transformations of stress components under reference system rotations. This makes exact replication of the standard material's oscillation impossible in most loading scenarios.

Spatial correlations in stress fields are best approximated by independently randomizing elastic parameters at discrete contacts, whereas introducing spatial dependence through spatial random fields with correlation lengths larger than particle size results in excessive stress spatial correlation compared to standard material.

Acknowledgement

Jan Eliáš and Jan Raisinger gratefully acknowledge financial support from the Czech Science Foundation under project number GA24-11845S and from project INODIN (Innovative methods of materials diagnostics and monitoring of engineering infrastructure to increase its durability and service time – CZ.02.01.01/00/23 020/0008487) co-funded by European Union. The former project financed the development of the homogenization technique and implementation of the RVE model, the latter was used to implement other material models and conduct the statistical study.

REFERENCES

[1] E. Schlangen und J. van Mier. "Simple lattice model for numerical simulation of fracture of concrete materials and structures". In: *Materials and Structures* 25 (1992), S. 534–542.

[2] E. Schlangen und E. Garboczi. "Fracture simulations of concrete using lattice models: Computational aspects". In: *Engineering Fracture Mechanics* 57.2 (1997), S. 319–332.

[3] Z. P. Bažant, M. R. Tabbara, M. T. Kazemi und G. Pijaudier-Cabot. "Random Particle Model for Fracture of Aggregate or Fiber Composites". In: *Journal of Engineering Mechanics* 116.8 (1990), S. 1686–1705.

[4] G. Cusatis, D. Pelessone und A. Mencarelli. "Lattice Discrete Particle Model (LDPM) for failure behavior of concrete. I: Theory". In: *Cement and Concrete Composites* 33.9 (2011), S. 881–890.

[5] T. Bhaduri, S. Gomaa und M. Alnaggar. "Coupled Experimental and Computational Investigation of the Interplay between Discrete and Continuous Reinforcement in Ultrahigh Performance Concrete Beams. II: Mesoscale Modeling". In: *Journal of Engineering Mechanics* 147.9 (2021), S. 04021050.

[6] T. Miura, H. Nakamura und Y. Yamamoto. "Expansive spalling mechanism of concrete due to high temperature based on developed hygro-thermal-mechanical model by 3D-RBSM-TNM". In: *Engineering Fracture Mechanics* 284 (2023), S. 109216.

[7] J. Mašek, J. Květoň und J. Eliáš. "Adaptive discretization refinement for discrete models of coupled mechanics and mass transport in concrete". In: *Construction and Building Materials* 395 (2023), S. 132243.

[8] Q. Zhang, J. Eliáš, K. Nagai und J. E. Bolander. "Discrete Modeling of Elastic Heterogeneous Media". In: *Mechanics*

Research Communications 137 (2024), S. 104277.

[9] J. E. Bolander, J. Eliáš, G. Cusatis und K. Nagai. “Discrete mechanical models of concrete fracture”. In: *Engineering Fracture Mechanics* 257 (2021), S. 108030.

[10] G. Cusatis und L. Cedolin. “Two-scale study of concrete fracturing behavior”. In: *Engineering Fracture Mechanics* 74.1 (2007). Fracture of Concrete Materials and Structures, S. 3–17.

[11] J. Eliáš. “Elastic properties of isotropic discrete systems: Connections between geometric structure and Poisson’s ratio”. In: *International Journal of Solids and Structures* 191-192 (2020), S. 254–263.

[12] G. Cusatis, R. Rezakhani und E. A. Schauffert. “Discontinuous Cell Method (DCM) for the simulation of cohesive fracture and fragmentation of continuous media”. In: *Engineering Fracture Mechanics* 170 (2017), S. 1–22.

[13] D. Asahina, K. Ito, J. Houseworth, J. T. Birkholzer und J. E. Bolander. “Simulating the Poisson effect in lattice models of elastic continua”. In: *Computers and Geotechnics* 70 (2015), S. 60–67.

[14] D. Asahina, K. Aoyagi, K. Kim, J. Birkholzer und J. Bolander. “Elastically-homogeneous lattice models of damage in geomaterials”. In: *Computers and Geotechnics* 81 (Jan. 2017), S. 195–206.

[15] K. Karhunen. *Zur Spektraltheorie stochastischer Prozesse*. Annales Academiae scientiarum Fennicae. 1946.

[16] P. D. Spanos und R. G. Ghanem. “Stochastic finite element expansion for random media”. In: *J. Eng. Mech., ASCE* 115.5 (1989), S. 1035–1053.

[17] G. Stefanou. “The stochastic finite element method: Past, present and future”. In: *Comp. Meth. Appl. Mech. Eng.* 198.2009 (2009), S. 1031–1051.

[18] H. Li, Z. Lü und X. Yuan. “Nataf transformation based point estimate method”. In: *Chin Sci Bull* 53.17 (2008), S. 2586–2592.